Numerical computation of invariant densities of linear control systems driven by multiplicative white noise

Fritz Colonius* Tobias Gayer† Iakovos Matsikis‡

March 31 2004

Abstract

For the 3-D linear oscillator with damping and disturbed by multiplicative white noise, we numerically compute the unique invariant density of the associated system obtained by projection onto the unit sphere. We show how varying feedback gains and noise intensities affect the corresponding density and consequently the stability properties.

1 Introduction

This paper presents a numerical study of linear feedback systems in $\mathbb{R}^d$ with multiplicative white noise of the form

$$\dot{x} = Ax + bu + \sigma\, A_1 x \circ dW(t) \tag{1}$$

$$y = c^T x \tag{2}$$

where $A, A_1 \in \mathbb{R}^{d\times d}$, $b, c \in \mathbb{R}^d$, σW is the Wiener process with intensity $\sigma \in \mathbb{R}$, and $\circ$ means that (1) is interpreted as a Stratonovich stochastic differential equation. Output feedback

$$u = -ky, \tag{3}$$

where $k \in \mathbb{R}$ is a gain parameter, yields the feedback system

$$dx = (A - kbc^T)x\, dt + \sigma\, A_1 x \circ dW(t)\,. \tag{4}$$

*Institut für Mathematik, Universität Augsburg, D-86135 Augsburg, Germany, colonius@math.uni-augsburg.de

†Institut für Mathematik, Universität Augsburg, D-86135 Augsburg, Germany, tobias.gayer@math.uni-augsburg.de

‡School of Mathematical Sciences, University of Exeter, Exeter EX4 4QE, UK, imat@maths.ex.ac.uk

It is well known that basic properties of this linear stochastic differential equation can be described by considering its projection to the unit sphere (or, more precisely, to projective space $\mathbb{P}^{d-1}$) and the corresponding invariant measure. In particular, this is true for the Lyapunov exponents (given by Khasminskii's formula). The purpose of the present paper is to present some results illustrating the influence of the gain parameter k and the intensity σ of the noise on the invariant measure. For a two dimensional system, Crauel/Matsikis/Townley [6] presented asymptotic results for high gain, i.e., for $k \to \infty$. For dimensions $d > 2$ the used expansion is not readily available. For $d = 3$, we will instead use a numerical approach for computation of the invariant measure on $\mathbb{P}^2$. In particular, we discuss the third order oscillators

$$\dddot{x} - a\ddot{x} - b\dot{x} - cx = u + \sigma x \circ dW \tag{5}$$

and

$$\dddot{x} - a\ddot{x} - b\dot{x} - cx = u + \sigma \dot{x} \circ dW, \tag{6}$$

with output feedback

$$u = -kx.$$

For the induced system on projective space $\mathbb{P}^2$, there is a unique invariant measure μ and it has support equal to $\mathbb{P}^2$. Using polar coordinates, we determine μ by discretisation of this space and simulation of the resulting Markov chain. This is done with the help of data structures provided by GAIO (Global Analysis of Invariant Objects), a program developed by M. Dellnitz, A. Hohmann, and O.Junge [8], [9]. Then the density of the invariant measure can be visualised (using MATLAB).

For deterministic systems it is well known that increasing the gain parameter k forces one, some, or even all of the eigenvalues to decrease relatively to the values of the gain. As a consequence the system will be pushed towards the eigendirection associated with the greatest positive eigenvalue (or least negative if all the eigenvalues become negative). A natural invariant measure for this system is a Dirac measure concentrated in this eigendirection.
The numerical simulations illustrate that this is also true for small noise intensity. Here the induced system on projective space will move faster and faster towards the least stable (or most unstable) eigendirection, hence the invariant measure will peak near this eigendirection. Increase of the noise intensity has an opposite effect: The invariant measure spreads out on projective space. Thus for higher noise intensity higher gains are necessary in order to obtain peaking near the least stable eigendirection (or, for smaller gains, less noise intensity is necessary in order to spread out the invariant measure).

The contents of the paper are as follows: In section 2 we recall results on the projected system on $\mathbb{P}^{d-1}$, in particular, the relevant Lie algebraic conditions. We verify that they are satisfied for (5) and (6) and indicate the parametrisation by polar coordinates.

Section 3 describes the numerical method. Section 4 illustrates this by application to a simple second order oscillator, and Section 5 presents results for the third order oscillators.

2 Projecting onto the unit sphere

In this section, we first recall some general results on Lyapunov exponents, that is, unique existence of invariant measures for the induced system on projective space and Lie algebraic conditions from Arnold, Oeljeklaus, Pardoux [5]. Then we verify that these Lie algebraic conditions are satisfied for the oscillators (5) and (6).

Consider a linear stochastic differential equation in $\mathbb{R}^d$ given by

$$dx_t = Ax_t\ dt + Dx_t \circ dW(t)$$

with $A, D \in \mathbb{R}^{d\times d}$. Defining

$$s = \frac{x}{|x|} \in \mathbb{S}^{d-1} := \{y \in \mathbb{R}^d,\ |y| = 1\},$$

this induces a (nonlinear) stochastic differential equation on the sphere $\mathbb{S}^{d-1}$ given by

$$ds = h_A(s)\, dt + h_D(s) \circ dW(t); \tag{7}$$

here $h_A(s) = As - (s, As)s$ and $h_D(s) = Ds - (s, Ds)s$. We note that this also induces a stochastic differential equation on projective space $\mathbb{P}^{d-1}$ which can be obtained by identifying opposite points on the sphere.

We cite the following theorem from [5]; see also Arnold [1], Theorem 6.2.16.

Theorem *: Suppose that the vector fields h_A and h_D induced by* (7) *on $\mathbb{S}^{d-1}$ satisfy the following hypoellipticity condition*

$$dim\ LA(h_A, h_D)(s) = d - 1, \quad for\ all\ s \in \mathbb{S}^{d-1}.$$

Then there exists a unique invariant measure on $\mathbb{P}^{d-1}$; it has a C^∞ density and the maximal Lyapunov exponent for (7) *is constant a.s.* □

Thus for the analysis of the oscillators (5) and (6) we have to verify the hypoellipticity condition. We first pass from (5) and (6) to the state space representation

$$dx = \begin{bmatrix} 0 & 1 & 0 \\ 0 & 0 & 1 \\ a & b & c-k \end{bmatrix} x\ dt + \sigma \begin{bmatrix} 0 & 0 & 0 \\ 0 & 0 & 0 \\ 0 & 0 & 1 \end{bmatrix} x \circ dW(t), \tag{8}$$

$$dx = \begin{bmatrix} 0 & 1 & 0 \\ 0 & 0 & 1 \\ a & b & c-k \end{bmatrix} x\ dt + \sigma \begin{bmatrix} 0 & 0 & 0 \\ 0 & 0 & 0 \\ 0 & 1 & 0 \end{bmatrix} x \circ dW(t). \tag{9}$$

Recall that a, b, c and k, σ are fixed real parameters.

Define

$$A = \begin{bmatrix} 0 & 1 & 0 \\ 0 & 0 & 1 \\ a & b & c-k \end{bmatrix},\ D_1 = \begin{bmatrix} 0 & 0 & 0 \\ 0 & 0 & 0 \\ 0 & 0 & 1 \end{bmatrix},\ D_2 = \begin{bmatrix} 0 & 0 & 0 \\ 0 & 0 & 0 \\ 0 & 1 & 0 \end{bmatrix}.$$

Then for $j = 1, 2$ the induced systems on $\mathbb{S}^2$ are given by

$$ds = h_A(s)\,dt + \sigma\ h_{D_j}(s) \circ dW(t) \tag{10}$$

and the hypoellipticity condition becomes

$$\dim\ LA(h_A, h_{D_j})(s) = 2 \quad \text{for all } s \in S^2.$$

Moreover the maximal Lyapunov exponent for (8) and (9) is given by Khasminskii's formula as

$$\lambda = \int_{\mathbb{S}^2} \left((s, As) + \frac{1}{2}((D_j + D_j^T)s, D_j s) - (s, D_j s)^2 \right) p(s) ds, \tag{11}$$

where $p(s)$ denotes the invariant density on $\mathbb{S}^2$, ds Lebesgue measure on $\mathbb{S}^2$ and D_j^T corresponds to the transpose matrix of D_j. A sufficient condition for uniqueness of the invariant measure is that the subspace generated by evaluating the corresponding linear vector fields in $\mathbb{R}^3$ have full dimensions. The following lemma shows that this is indeed the case.

2.1 Lemma *Suppose that for the systems* (8) *and* (9) *the coefficient* $a \neq 0$. *Then for* $j = 1, 2$ *and every* $x \in \mathbb{R}^3 \backslash \{0\}$

$$\dim\ LA\{Ax, D_j x\}(x) = 3.$$

Proof: We first treat the case $LA\{Ax, D_1 x\}$ where the vector fields Ax and $D_1 x$ are given by

$$Ax = \begin{pmatrix} x_2 \\ x_3 \\ ax_1 + bx_2 + (c-k)x_3 \end{pmatrix},\ D_1 x = \begin{pmatrix} 0 \\ 0 \\ x_3 \end{pmatrix}. \tag{12}$$

We compute the Lie bracket

$$[Ax, D_1 x] = (D_1 A - A D_1)x = \begin{pmatrix} 0 & 0 & 0 \\ 0 & 0 & -1 \\ a & b & 0 \end{pmatrix} x = \begin{pmatrix} 0 \\ -x_3 \\ ax_1 + bx_2 \end{pmatrix}.$$

Thus for $x_2 \neq 0$ and $x_3 \neq 0$ the span is equal to $\mathbb{R}^3$. We further compute

$$\begin{aligned} [Ax, [Ax, D_1 x]] = [A, [A, D_1]]x &= ([A, D_1]A - A[A, D_1])\,x \\ &= \begin{pmatrix} 0 & 0 & 1 \\ -2a & -2b & -(c-k) \\ -a(c-k) & a - b(c-k) & 2b \end{pmatrix} x \\ &= \begin{pmatrix} x_3 \\ -2ax_1 - 2bx_2 - (c-k)x_3 \\ -a(c-k)x_1 - (b(c-k) - a)x_2 + 2bx_3 \end{pmatrix}. \end{aligned}$$

If $x_1 = x_2 = 0$, then $x_3 \neq 0$, since $x \in \mathbb{R}^3 \setminus \{0\}$. Hence (12) and the Lie bracket above yield three independent directions. Analogously, the assertion follows if $x_1 = x_3 = 0$. It remains to discuss the case $x_2 = x_3 = 0$, and hence $x_1 \neq 0$.

Since $a \neq 0$, Ax and the Lie bracket above provide two independent directions. In order to find a third independent direction we compute

$$[A,[A,[A,D_1]]] = \begin{pmatrix} 3a & 3b & 2(c-k) \\ 0 & -3a & -4b-(c-k)^2 \\ 4ab+a(c-k)^2 & 4b^2-2a(c-k)+b(c-k)^2 & 0 \end{pmatrix}$$

and hence

$$[A,[A,[A,D_1]]](x) = \begin{pmatrix} -3ax_1-3bx_2-2(c-k)x_3 \\ 3ax_2+(4b+(c-k)^2)x_3 \\ -4abx_1+(-4b^2+2a(c-k)-b(c-k)^2)x_2 \end{pmatrix}.$$

This provides a direction independent of Ax and $[A,[A,D_1]]x$. This proves the first part of the lemma.
We proceed in exactly the same manner for the second case involving the diffusion matrix D_2; here

$$Ax = \begin{pmatrix} x_2 \\ x_3 \\ ax_1+bx_2+(c-k)x_3 \end{pmatrix}, \; D_2x = \begin{pmatrix} 0 \\ 0 \\ x_2 \end{pmatrix}.$$

We compute the first bracket of A and D_2 as

$$[A,D_2]x = (D_2A - AD_2)x = \begin{pmatrix} 0 \\ -x_2 \\ -(c-k)x_2+x_3 \end{pmatrix}.$$

These three vectors provide us with three independent directions, as long as $x_2 \neq 0$. If $x_2 = 0$ and $x_3 \neq 0$, we have the two independent directions.

$$\begin{pmatrix} 0 \\ x_3 \\ ax_1+(c-k)x_3 \end{pmatrix}, \quad \begin{pmatrix} 0 \\ 0 \\ x_3 \end{pmatrix}.$$

If $x_2 = x_3 = 0$, we only have the direction

$$Ax = \begin{pmatrix} 0 \\ 0 \\ ax_1 \end{pmatrix}.$$

We further compute

$$[A,[A,D_2]]x = \begin{pmatrix} x_2 \\ (c-k)x_2-2x_3 \\ ax_1+(2b+(c-k)^2)x_2-(c-k)x_3 \end{pmatrix}$$

and

$$[A,[A,[A,D_2]]]x = \begin{pmatrix} -(c-k)x_2 + 3x_3 \\ -3ax_1 - (4b + (c-k)^2)x_2 \\ -2a(c-k)x_1 - (4b(c-k) + (c-k)^3)x_2 + (4b + (c-k)^2)x_3 \end{pmatrix}, \tag{13}$$

and, finally,

$$[A,[A,[A,[A,D_2]]]]x = \begin{pmatrix} 6ax_1 + (7b + (c-k)^2)x_2 + 2(c-k)x_3 \\ z_1x_1 + z_2x_2 - z_3x_3 \\ y_1x_1 + y_2x_2 - y_3x_3 \end{pmatrix}, \tag{14}$$

where $z_1 = 2a(c-k)$, $z_2 = (4b(c-k) + (c-k)^3 - 3a)$, $z_3 = (8b + 2(c-k)^2)$, $y_1 = (7ab + 3a(c-k)^2)$, $y_2 = (-a(c-k) + 8b^2 + 6b(c-k)^2 + (c-k)^4)$, $y_3 = (3a + 4b(c-k) + (c-k)^3)$.

If $x_2 = x_3 = 0$, then, in addition to Ax, we obtain the two independent directions (13) and (14).

The case $x_2 = 0, x_3 \neq 0$ is covered from the directions given by Ax, $[A, D_2]x$ and $[A,[A,[A,D_2]]]x$. This completes the proof.

□

This lemma, together with the theorem cited above shows that the induced equations on projective space possess unique invariant measures. The C^∞ densities associated with these measures can be obtained as suitably normalised solutions of the corresponding Fokker-Planck equations in projective space. In some cases (for $d = 2$) this even admits an analytical description, see [6]. In general, one may use numerical procedures for partial differential equations to solve the Fokker-Planck equation.
Below we follow another numerical approach based on discretising the state space and then using a Monte-Carlo approach. It will be convenient to introduce angular coordinates for the considered systems in $\mathbb{S}^1$ and $\mathbb{S}^2$.

For the stochastic differential equations (10) we get

$$h_A(s) = \begin{pmatrix} s_2 - s_1(s, As) \\ s_3 - s_2(s, As) \\ as_1 + bs_2 + (c-k)s_3 - s_3(s, As) \end{pmatrix},$$

and

$$h_{D_1}(s) = \sigma \begin{pmatrix} -s_1(s, D_1s) \\ -s_2(s, D_1s) \\ s_3 - s_3(s, D_1s) \end{pmatrix}, \; h_{D_2}(s) = \sigma \begin{pmatrix} -s_1(s, D_2s) \\ -s_2(s, D_2s) \\ s_2 - s_3(s, D_2s) \end{pmatrix},$$

with

$$(s, As) = s_1s_2 + s_2s_3 + as_3s_1 + bs_3s_2 + (c-k)s_3^2,$$
$$(s, D_1s) = s_3^2 \text{ and } (s, D_2s) = s_3s_2.$$

On the unit sphere the Cartesian coordinates are $s = (s_1, s_2, s_3)^T$ and changing to angular coordinates $s = (\cos\phi\sin\theta, \sin\phi\sin\theta, \cos\theta)^T$ with $\phi \in [0, 2\pi)$ and $\theta \in [0, \pi/2)$ (where $\theta \in [0, \pi/2)$, since the density is periodic; the lower half of the unit sphere can be recovered by multiplying with -1), gives

$$d\theta = -\frac{ds_3}{\sin\theta},\ d\phi = \frac{ds_2}{\sin\theta\cos\phi} - \cot\theta\tan\phi d\theta.$$

These equations produce the final transformation, with respect to the angles θ and ϕ, of equations (10) with $j = 1, 2$. Abbreviate

$$\begin{aligned} M_A = &\sin^2\theta\cos\phi\sin\phi + a\sin\theta\cos\phi\cos\theta \\ &+ (1+b)\sin\theta\sin\phi\cos\theta + (c-k)\cos^2\theta. \end{aligned}$$

We compute for $j = 1$

$$\begin{aligned} d\theta = &-\Big(a\cos\phi + b\sin\phi + (c-k)\cot\theta - \cot\theta M_A\Big)dt \\ &- \sigma\Big(\cot\theta - \cot\theta\cos^2\theta\Big) \circ dW(t), \end{aligned}$$

$$\begin{aligned} d\phi = &\Big(\frac{\cot\theta}{\cos\phi} - \tan\phi M_A + a\cot\theta\sin\phi \\ &+ b\frac{\cot\theta\sin^2\phi}{\cos\phi} + (c-k)\cot^2\theta\tan\phi - \cot^2\theta\tan\phi M_A\Big)dt \\ &- \sigma\Big(\tan\phi\cos^2\theta - \cot^2\theta\tan\phi + \cot^2\theta\tan\phi\cos^2\theta\Big) \circ dW(t) \end{aligned}$$

and for $j = 2$ we similarly find

$$\begin{aligned} d\theta = &-\Big(a\cos\phi + b\sin\phi + (c-k)\cot\theta - \cot\theta M_A\Big)dt \\ &- \sigma\Big(\sin\phi - \sin\phi\cos^2\theta\Big) \circ dW(t), \end{aligned}$$

$$\begin{aligned} d\phi = &\Big(\frac{\cot\theta}{\cos\phi} - \tan\phi M_A + a\cot\theta\sin\phi \\ &+ b\frac{\cot\theta\sin^2\phi}{\cos\phi} + (c-k)\cot^2\theta\tan\phi - \cot^2\theta\tan\phi M_A\Big)dt \\ &- \sigma\Big(\frac{\sin\theta\sin^2\phi\cos\theta}{\cos\phi} - \frac{\cot\theta\sin^2\phi}{\cos\phi} + \frac{\sin^2\phi\cos^3\theta}{\sin\theta\cos\phi}\Big) \circ dW(t). \end{aligned}$$

3 Numerical Approximation of the Invariant Densities

In this section we discuss a numerical method for approximating the unique invariant density in projective space.

We first discretise the state space by dividing it into 'boxes'. For the projected system in $\mathbb{S}^2$ we use angular coordinates. Identifying opposite points on the sphere we obtain the projective space $\mathbb{P}^2$. For this space we use coordinates in $K = [0, 2\pi] \times [0, \frac{\pi}{2}]$ which is the upper half of the unit sphere. The computation of the invariant density on this space is based on the discretisation of the Frobenius-Perron operator defined on the space of probability measures on $\mathbb{R}^2$. Choose a discretisation time $T > 0$ and define a partition $\mathcal{P}$ of K into finitely many boxes B_i. Then compute the transition probabilities

$$p_{ij} := \frac{1}{m(B_i)} \int_{B_i} P(T, x, B_j)\, dx$$

for the ensuing discretised system averaged over the box covering. Here $m(\cdot)$ denotes the Lebesgue measure. The transition matrix $P := (p_{ij}) \in \mathbb{R}^{(N+1)\times(N+1)}$ is row stochastic.

For a convenient generation of the partition and the boxes we rely on numerical methods in Szolnoki [16] based on subdivision techniques for the numerical analysis of dynamical systems developed by Dellnitz, Hohmann, and Junge (see [7], [8]). For the approximation of the dynamics on this box partition, we create a Markov chain with finitely many states each of which symbolises one box. The transition probabilities from one state to the other are computed by Monte Carlo simulation; here we use a stochastic Runge-Kutta technique of order four; see, e.g., Kloeden/Platen [14].

More specifically, s_2 starting points x^k are picked in each box B_i. From each starting point, the solution is approximated for all samples $\hat{\eta}^l$ generating $s_1 s_2$ target points $\hat{\varphi}(T, x^k, \hat{\eta}^l)$. The transition function from box B_i to B_j is then approximated by

$$p_{ij} = \frac{1}{m(B_i)} \int_{B_i} P(T, x, \eta_t) dx \approx \frac{1}{s_1 s_2} \sum_{l}^{s_1} \sum_{k}^{s_2} \chi_{B_j} \left(\hat{\varphi}(T, x^k, \hat{\eta}^l) \right).$$

The question as to how many starting points, boxes, and sample paths of the background process should be used depends on the properties of the system, the time length T, and the box size—and of course on the available computing resources.

This yields the transition matrix of the Markov chain, which in its turn allows the computation of the stationary density which is represented as a normalised eigenvector of the discretised Frobenius-Perron operator associated with the eigenvalue one. Thus an approximation to a fixed point of the Frobenius-Perron operator is obtained.

3.1 Remark The universally applied idea of Monte Carlo simulations goes back to Ulam, Metropolis, and von Neumann (see [15]). Although many sophisticated variants for different disciplines have been developed in the meanwhile, there are no general error estimates available. So one can never be sure that the Monte Carlo simulation recognises every relevant behaviour.

3.2 Remark For further information on results concerning the convergence of the above approximations we refer the reader to [8], [11], [10] for the deterministic case and to [12] for the approximation of invariant measures for random dynamical systems.

4 Examples, 2-D case

In this section we illustrate the previous ideas for the following two dimensional stochastic oscillator with noise acting in a purely skew symmetric way:

$$dx = \begin{pmatrix} 3-k & -4 \\ 1 & -10 \end{pmatrix} x dt + \sigma \begin{pmatrix} 0 & -1 \\ 1 & 0 \end{pmatrix} x \circ dW(t). \tag{15}$$

Specifically we will study the effects of small ($\sigma = 10^{-5}$) and relatively big ($\sigma = 1$) noise, on the corresponding invariant measure of (15), for different high gain values.
We adopt the values $a = 3, b = -4, c = 1, d = -10$ for the drift matrix (which we call A_1) because they make the origin of the unperturbed system a saddle and the corresponding root locus is dynamically more interesting.

4.1 Remark Observe that when noise enters in this skew symmetric way the system for the angle ϕ on $\mathbb{S}^1$ is elliptic and so there is a unique invariant measure.

4.1 Small noise intensity

We start by plotting the root locus for the unperturbed equation (15). This is shown in Figure 1.

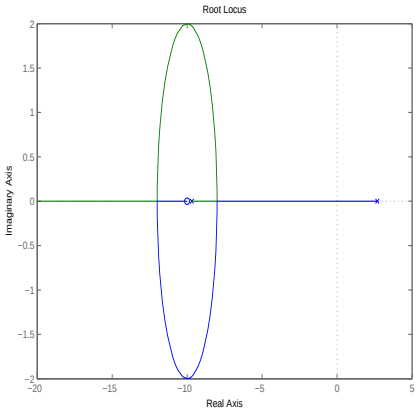

Fig.1 : Root locus for A_1.

The root locus shows that for $0 < k \leq 9$ there are two real eigenvalues $\lambda_1 \approx -9.69$ and $\lambda_2 \approx 2.69$, which become complex for $9 < k < 17$ and eventually for $k \geq 17$ one converges to minus infinity and the other to $d = -10$. Thus the origin will change from being a saddle, to a stable spiral, and eventually will become a stable node.
The latter arguments imply that the invariant measure of (15) for $0 < k \leq 9$ will almost be a Dirac measure concentrated in the eigendirection corresponding to λ_2; this is shown in Figure 2. (*Here and in the following figures we plot the different values of the density as distances from the unit circle* $\mathbb{S}^1$). For $9 < k < 17$ the density assumes positive values in a wider area, since the solution becomes a spiral and thus visits some areas of $\mathbb{S}^1$

more often (Figure 3). However, since noise is small, high gain forces the density to concentrate more in one 'box'. This is seen in Figure 3 where only one big peak appears.

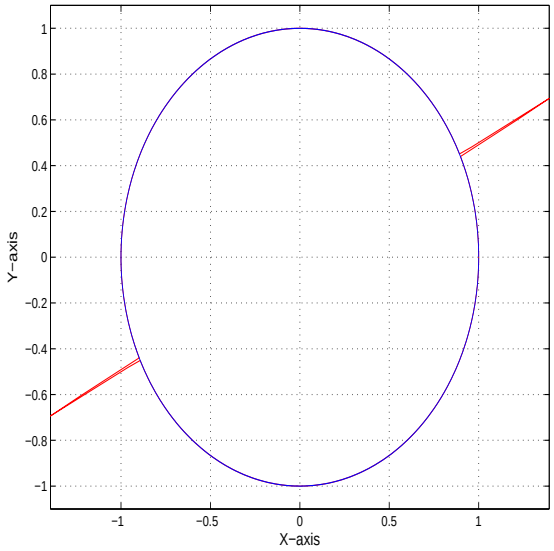

Fig.2: $\sigma = 10^{-5}$ and $k = 9$

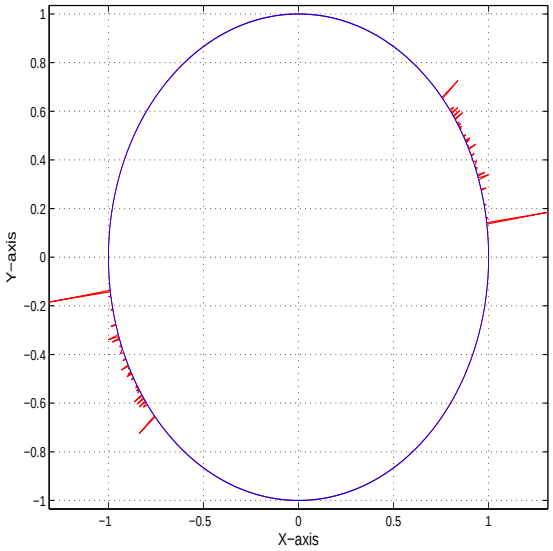

Fig.3: $\sigma = 10^{-5}$ and $k = 10$

For $k = 20$, the measure returns to being almost Dirac, Figure 4. Increasing k further, noise gradually loses its effect and the measure approximates a Dirac measure concentrated on the north pole, Figure 5.

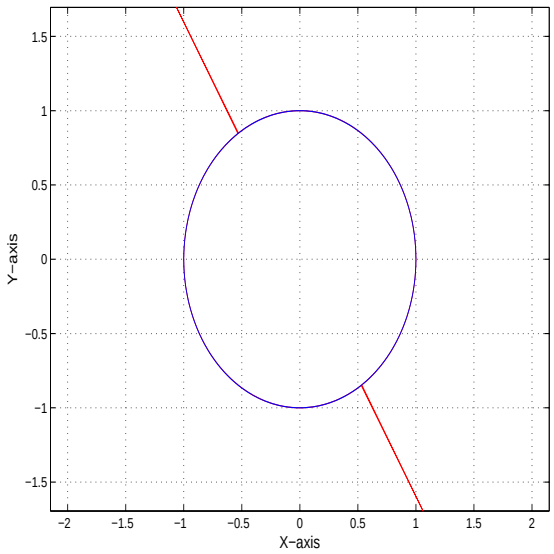

Fig.4: $\sigma = 10^{-5}$ and $k = 20$

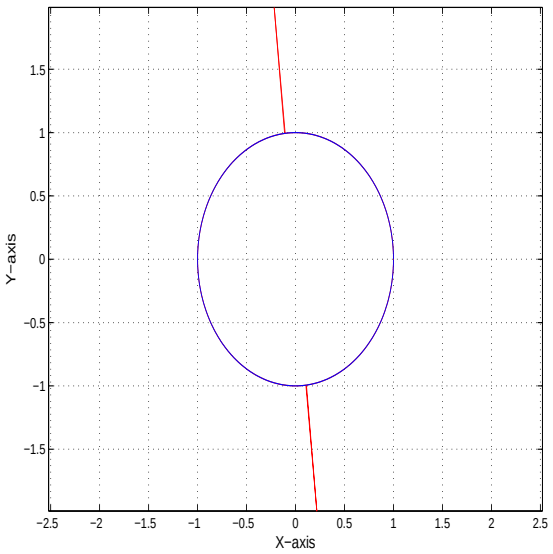

Fig.5: $\sigma = 10^{-5}$ and $k = 50$

4.2 Noise intensity $\sigma = 1$

In this subsection we treat again equation (15), but we increase the noise intensity to one. The smoothing effect of noise can be viewed in the following two figures which were

made using the same configuration as for Figures 3 and 5, with the exception that noise intensity was increased.

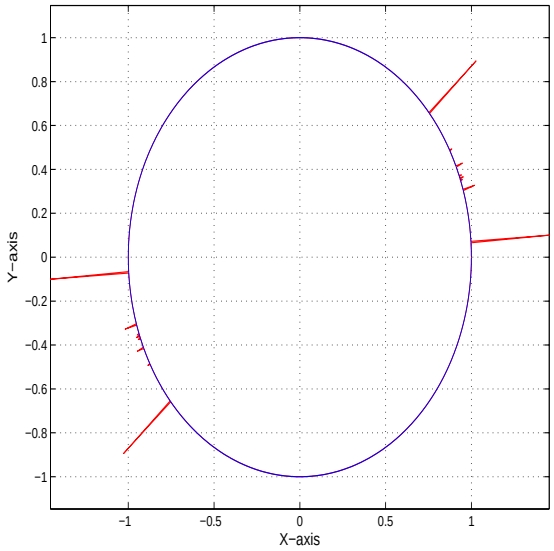

Fig.6: $\sigma = 1$ and $k = 10$

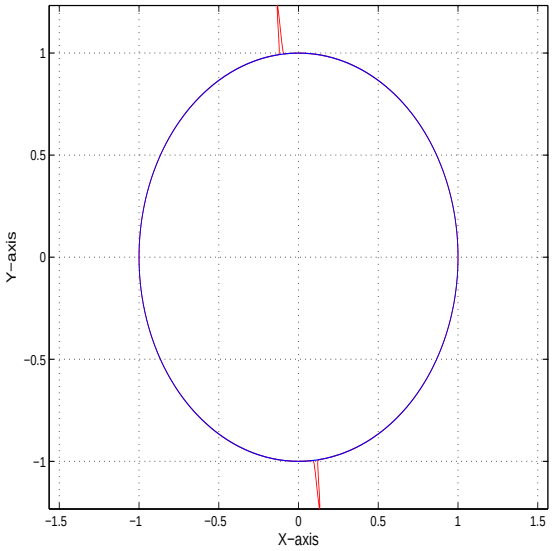

Fig.7: $\sigma = 1$ and $k = 50$

Observe how the density from peaking at one point in Figure 3, 'spreads out' in two big peaks in Figure 6. The same happens between Figures 5 and 7 where the peak from having value almost one for $\sigma = 10^{-5}$ becomes much smaller and spreads uniformly on the surface of $\mathbb{S}^1$.

5 Examples, 3-D case

We now study the combined effect of noise intensity and high gain on the density of the third order linear oscillators (5) and (9). For both equations the drift matrices A coincide. We begin with the root locus of the drift matrix A. Then we study (5) and (9) considering different noise intensities and gains k.

Note: *In contrast to the 2-D case where we plotted the different density values as distances from the surface of* $\mathbb{S}^1$*, here we use colour to plot them on* $\mathbb{S}^2$*. So in the figures that follow we use different colour intensities, with red being the highest, to plot the density values on* $\mathbb{S}^2$*.*

5.1 Small noise intensity

The root locus for the drift matrix

$$A = \begin{pmatrix} 0 & 1 & 0 \\ 0 & 0 & 1 \\ -5 & 2 & 3-k \end{pmatrix}$$

is plotted in Figure 8.

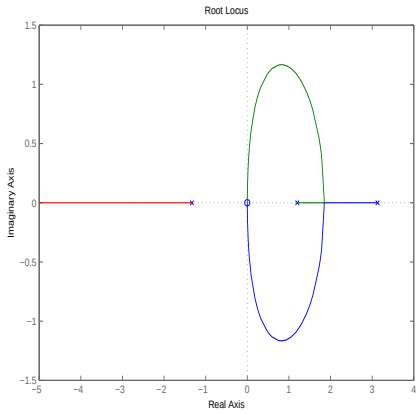

Fig.8 : Root locus for A.

In particular, for $k = 0$ we get three real eigenvalues $\lambda_1 = 3.1284, \lambda_2 = -1.3301$ and $\lambda_3 = 1.2016$. The red line indicates that λ_2 will remain real for all subsequent values of k and will move gradually towards minus infinity. On the other hand, when $k \approx 0.77$ the eigenvalues λ_1 and λ_3 become complex and stay complex for all greater values of k. Next we study equation (5) given by

$$dx = \begin{pmatrix} 0 & 1 & 0 \\ 0 & 0 & 1 \\ -5 & 2 & 3-k \end{pmatrix} x\ dt + \sigma \begin{pmatrix} 0 & 0 & 0 \\ 0 & 0 & 0 \\ 0 & 0 & 1 \end{pmatrix} x \circ dW(t). \tag{16}$$

Thus for $k = 0$ we get an 'almost' Dirac measure concentrated in the eigendirection associated with λ_1; this can be seen in Figure 9. For $k > 0.77$ the solution of the unperturbed system becomes an unstable spiral and so the peak flattens in Figure 10.

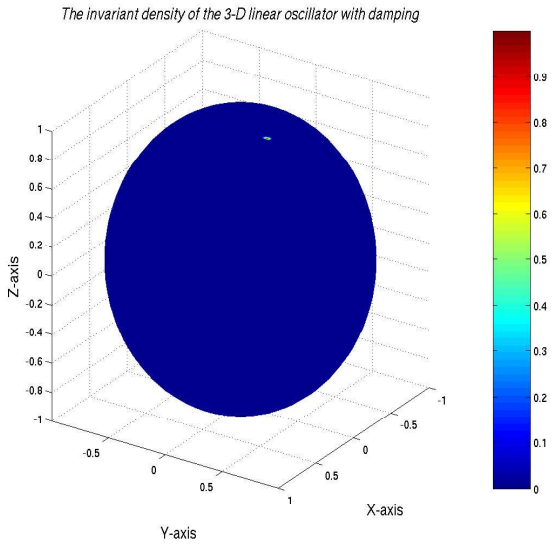

Fig.9: $\sigma = 10^{-6}$ and $k = 0$

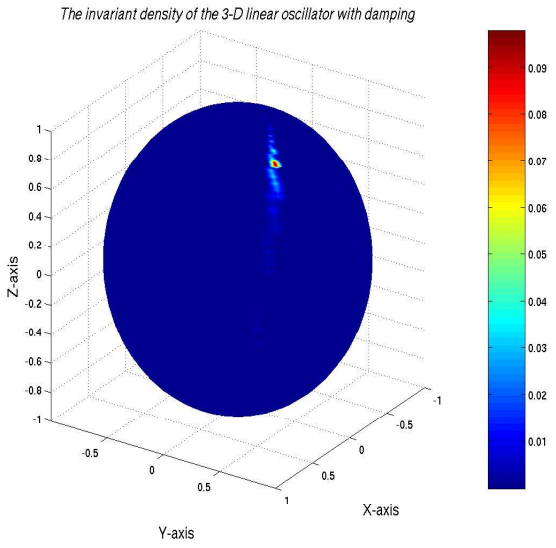

Fig.10: $\sigma = 10^{-6}$ and $k = 1$

Increasing now k to values higher than one forces the solution to oscillate faster since the imaginary parts of λ_1 and λ_3 increase. Therefore the density becomes a 'ring' around $\mathbb{S}^2$ as can be seen in Figures 11 and 12.

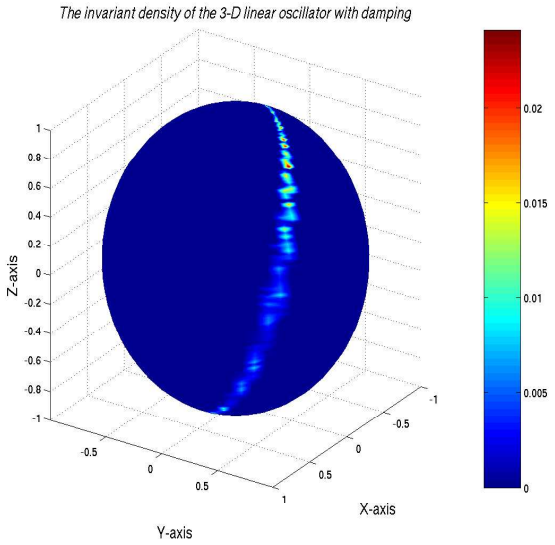

Fig.11: $\sigma = 10^{-6}$ and $k = 3$

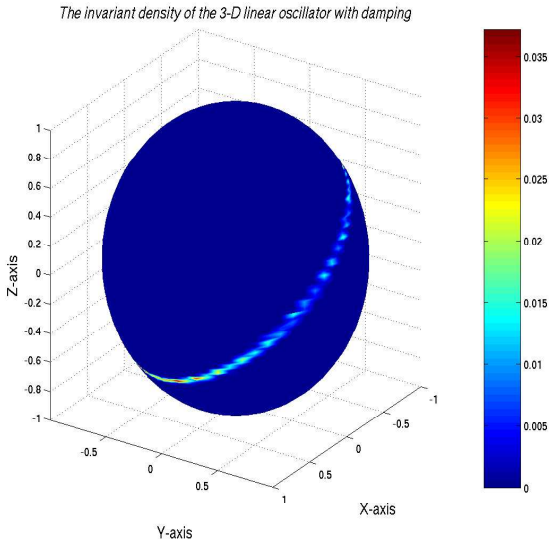

Fig.12: $\sigma = 10^{-6}$ and $k = 10$

For $k > 10$ the density will keep on being a 'ring' and eventually become the equator. Observe, however, that for higher values of k the noise affects the system less and so the density concentrates (peaks) more. This is seen in Figure 12 where the red highlighted area assumes values close to 0.04, in comparison with 0.03 in Figure 11.

5.2 Higher Noise Intensity

We now increase the noise intensity to $\sigma = 1$ and compare with the small noise case. Observe in Figures 13, 14, 15, and 16 how the density spreads out in comparison with the small intensity case. The peaks for example in Figures 11 and 12 disappear.

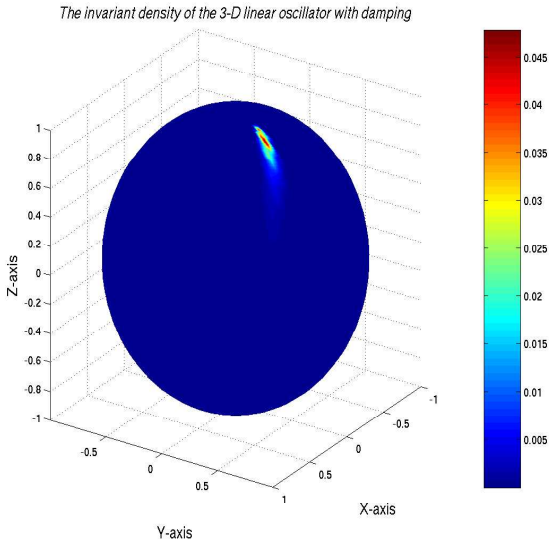

Fig.13: $\sigma = 1$ and $k = 0$

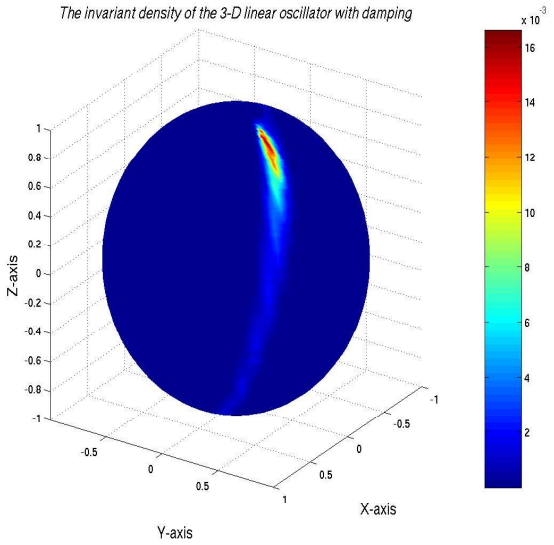

Fig.14: $\sigma = 1$ and $k = 1$

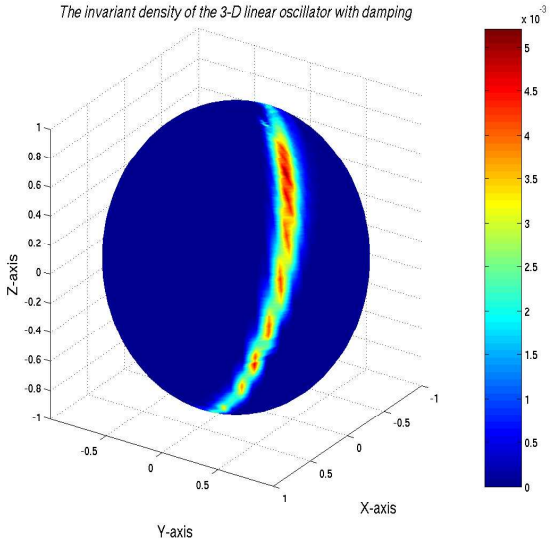

Fig.15: $\sigma = 1$ and $k = 3$

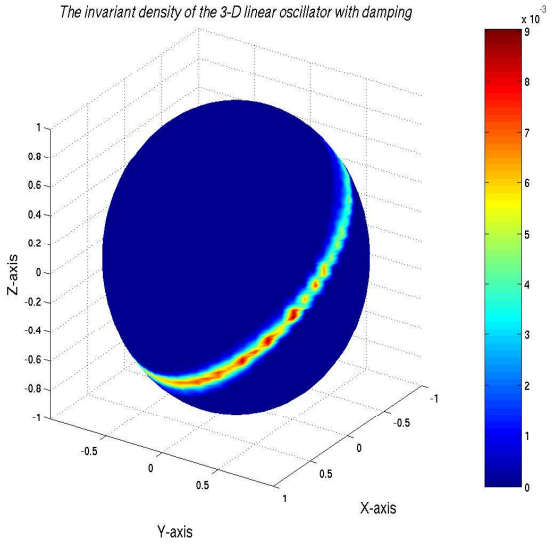

Fig.16: $\sigma = 1$ and $k = 10$

Before closing this subsection we present two more figures, one for $\sigma = 5$ and one for $\sigma = 20$, where the smoothing effect of higher noise intensity becomes more visible.

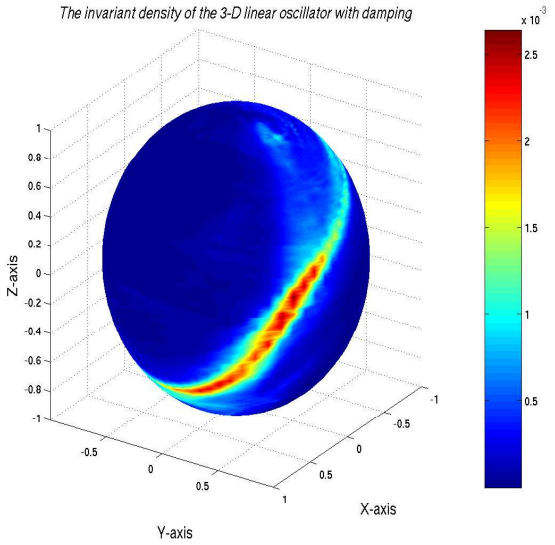

Fig.17: $\sigma = 5$ and $k = 10$

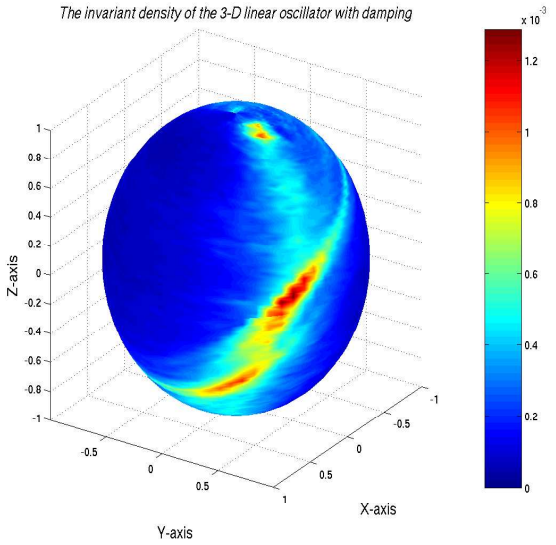

Fig.18: $\sigma = 20$ and $k = 10$

Clearly the more σ increases while k remains the same, the density flattens more around the sphere in a uniform manner.

5.3 Different diffusions

Finally, we study what happens to the density function when we switch from equation (8) to equation (9). We use the same drift matrix A for the calculations and noise intensity $\sigma = 5$.

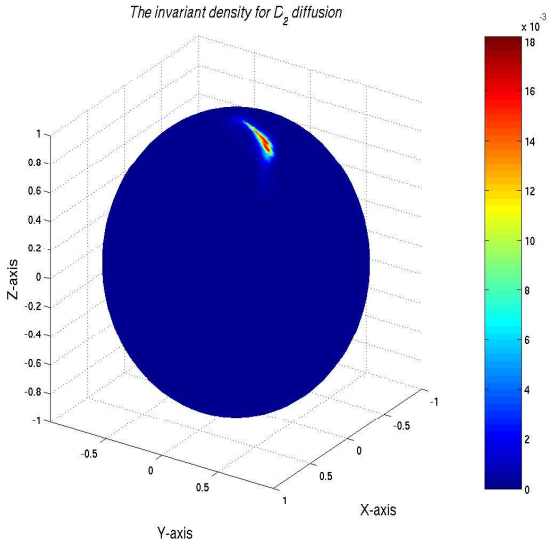

Fig.19: $\sigma = 1$ and $k = 0$

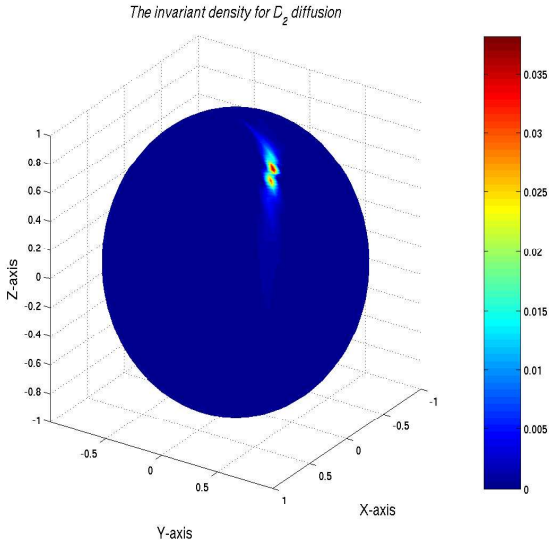

Fig.20: $\sigma = 1$ and $k = 1$

We see that although the quantitative behaviour of the density remains the same, as can be easily seen between Figures 13,14 and 19,20, nevertheless qualitatively the density

finds a new area of concentration, Figures 15,16 and 21,22. This lead us to believe that different mixing of noise alters significantly the properties of the invariant measure when high gain is not big enough to counterbalance the effect of the noise.

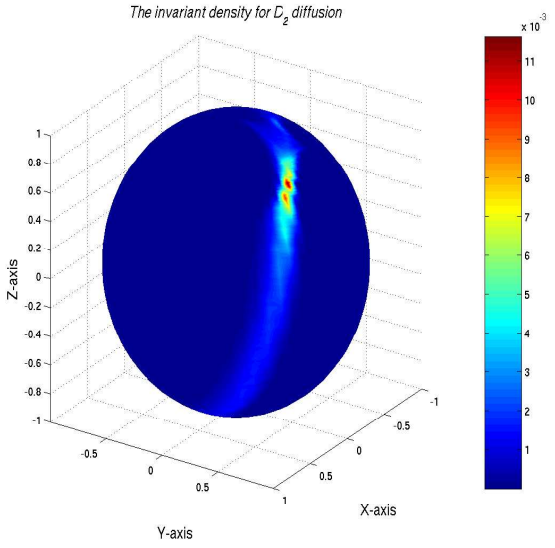

Fig.21: $\sigma = 1$ and $k = 3$

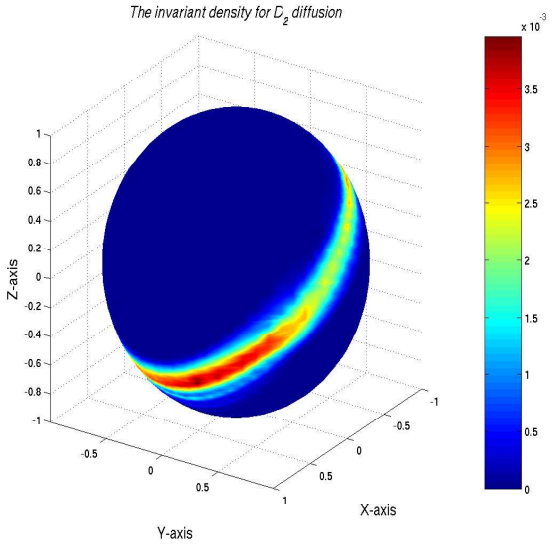

Fig.22: $\sigma = 1$ and $k = 10$

5.4 Application to Lyapunov exponents

Using the measures we calculated in the previous section, we now compute the Lyapunov exponents λ_{D_1} and λ_{D_2} from equation (11) as functions of high gain and noise intensity. Specifically we plot λ_{D_1,D_2} for $0 \leq k \leq 10$ and for noise intensities $\sigma = 10^{-6}$ and $\sigma = 1$. We start by computing for equation (8) the maximal Lyapunov exponent (11) with respect to the angles (ϕ, θ) on $\mathbb{P}^2$. This gives

$$\lambda_{D_1} = \int_0^{2\pi} \int_0^{\frac{\pi}{2}} (\frac{1}{2}\sin 2\phi \sin^2\theta + \frac{1}{2}\sin 2\theta(\sin\phi + a\cos\phi + b\sin\phi) + (c-k)\cos^2\theta + \sigma^2(\cos^2\theta \sin^2\theta)\ p(\phi,\theta)d\phi d\theta.$$

Using equation (11) but with different diffusion D_2, we recover the following integral whose solution gives the greatest Lyapunov exponent of equation (9) :

$$\lambda_{D_2} = \int_0^{2\pi} \int_0^{\frac{\pi}{2}} (\frac{1}{2}\sin 2\phi \sin^2\theta + \frac{1}{2}\sin 2\theta(\sin\phi + a\cos\phi + b\sin\phi) + (c-k)\cos^2\theta + \frac{\sigma^2}{2}(\sin^2\phi \sin^2\theta - 2\cos^2\theta \sin^2\phi \sin^2\theta))\ p(\phi,\theta)d\phi d\theta.$$

In the following figures blue colour corresponds to λ_{D_1} and λ_{D_2} and red to the real parts A, the drift matrix of equations (8) and (9). Both exponents are plotted as k is being increased with a step of 1 from zero to ten.

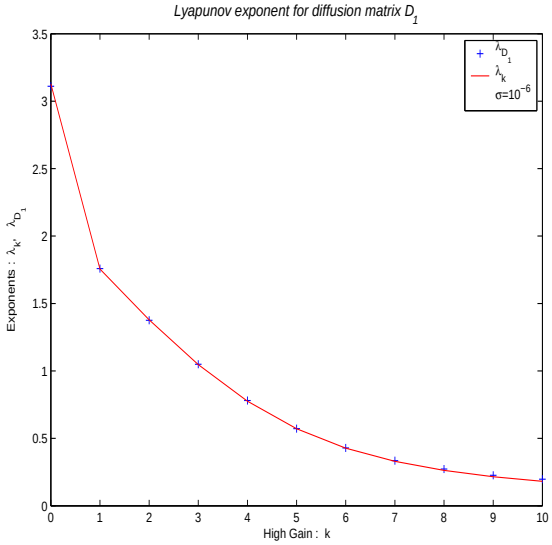

Fig.23: $\lambda_{D_1},\ \sigma = 10^{-6}$

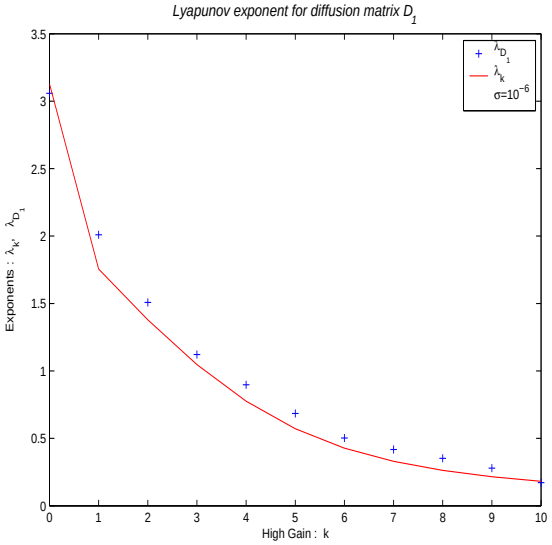

Fig.24: $\lambda_{D_1},\ \sigma = 1$

Clearly when σ is small λ_{D_1} (and λ_{D_2}) matches the deterministic exponent, Figure 23. Increasing the noise intensity has a destabilising effect on the system as can be viewed in Figure 24, where λ_{D_1} instead of converging fast towards zero is forced to remain positive for a longer period. λ_{D_2} assumes smaller values than the deterministic maximal exponent since the diffusion part coming from D_2 in the Khasminskii formula contributes negative values. So when noise enters with diffusion D_2 stabilises in contrast to D_1.
Nevertheless both λ_{D_1} and λ_{D_2} converge to the deterministic exponent as greater k. This is expected, as the invariant measure converges to its deterministic counterpart while k increases.

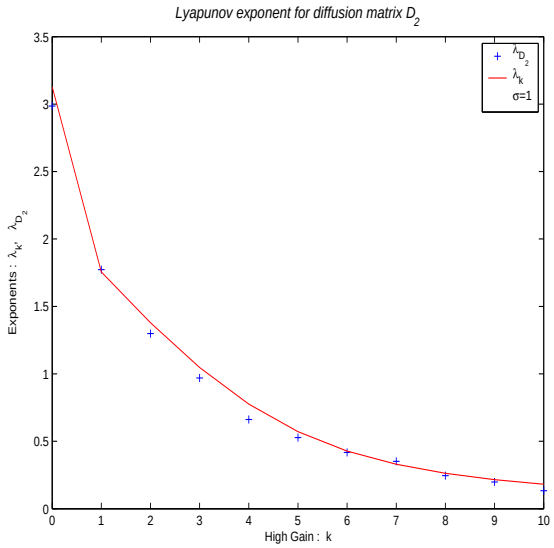

Fig.25: $\lambda_{D_2},\ \sigma = 1$

6 Acknowledgements

We would like to thank Hans Crauel, Technical University of Ilmenau and Stuart Townley, University of Exeter, for their various comments and suggestions. Iakovos Matsikis was supported by CTS (European, Control Training Site) in the form of a fellowship.

References

[1] L. Arnold, *Random Dynamical Systems*, Springer-Verlag, 1998.

[2] L. Arnold, H. Crauel, and V. Wihstutz, Stabilisation of linear systems by noise, *SIAM J. Control Optimisation* 21 (1983), pp. 451–461.

[3] L. Arnold, A. Eizenberg, and V. Wihstutz, Large noise asymptotics of invariant measures, with applications to Lyapunov exponents, *Stochastics Stochastics Rep.* 59 (1996), pp. 71–142.

[4] L. Arnold, W. Kliemann, and E. Oeljeklaus, Lyapunov exponents of linear stochastic systems, in L- Arnold, V. Wihstutz, editors, *Lyapunov Exponents, Proceedings, Bremen 1984*, Springer-Verlag *1986,* pp. 85–125.

[5] L. Arnold, E. Oeljeklaus, and E. Pardoux, Almost sure and moment stability for linear Itô equations, in *Lyapunov Exponents, Proceedings, Bremen 1984* , Springer-Verlag *1986,* pp. 129–159.

[6] H. Crauel, I. Matsikis, and S. Townley, Almost sure and second mean high gain stabilisation, in *SIAM J. Control Optimisation* Vol.42, No 5, pp. 1834-1853.

[7] M. Dellnitz, A. Hohmann, *A subdivision algorithm for the computation of unstable manifolds and global attractors*, *Numer. Math.* **75** (1997), 293–317.

[8] M. Dellnitz, O. Junge, *Set oriented numerical methods for dynamical systems*, in B. Fiedler, G. Iooss, N. Kopell (eds.), *Handbook of Dynamical Systems III: Towards Applications*, (World Scientific, 2002) 221–264.

[9] M. Dellnitz, A. Hohmann, O. Junge and M. Rumpf, Exploring invariant sets and invariant measures,*CHAOS:An Interdisciplinary Journal of Nonlinear Science*, **7**(2), 1997.

[10] J. Ding, Q. Du, T.Y. Li, High Order Approximation of the Frobenius-Perron Operator, *Applied Mathematics and Computation* 53(1993), pp. 151-171.

[11] F.Y. Hunt, A Monte Carlo Approach to the Approximation of Invariant measures, National Institute of Standards and Technology, *NISTIR* **4980**, (1993).

[12] P. Imkeller, P. Kloeden, On the computation of invariant measures in random dynamical systems, *Stochastics and Dynamics*, Vol.3, No.2, (2003), pp. 247-265.

[13] A. Isidori, *Nonlinear Control Systems*, Springer-Verlag, 1994.

[14] P. Kloeden, E. Platen, *Numerical Solution of Stochastic Differential Equations*, Springer-Verlag, Berlin Heidelberg 1992.

[15] N. Metropolis, S. Ulam, *The Monte Carlo method*, *J. Amer. Statist. Assoc.* **44** (247) (1949), 335–341.

[16] D. Szolnoki, *Set oriented methods for computing reachable sets and control sets*, *Discrete Contin. Dynam. Systems–B* **3** (2003), 361–382.